ELSEVIER

Polymer 41 (2000) 4233–4248

polymer

Comparative crystallisation and exploratory microstructure studies of novel polyethylenes with tailored molecular characteristics

J.J. Janimak*, G.C. Stevens[1]

Polymer Research Centre, University of Surrey, Guildford, Surrey GU2 5XH, UK

Received 11 March 1999; accepted 20 August 1999

Abstract

As part of a long-term project aimed at understanding chromium and metallocene catalysed polyolefins, we are seeking to establish a fundamental understanding of structure–property–processing relationships through the control of molecular variables. Through careful selection of polyethylene materials with different molecular weight distributions, level of short chain branching and catalyst type we have been exploring some of these objectives. All our polyethylenes are centred on medium density materials but they differ with respect to molecular variables.

Crystallisation kinetics of these materials were studied under isothermal conditions and evaluation of their behaviour has been extrapolated from classical Avrami analysis. By studying the crystallisation kinetics in parallel with melting behaviour, we have been able to correlate thermal transition changes with underlying lamellar characteristics obtained from electron microscopy. This approach allows the distribution of lamellae, thermal stability and molecular constitution to be mapped in real space.

In melt-crystallised lamellae, a three tier morphological profile was identified in both chromium and metallocene catalysed polyethylenes. Banded spherulitic structures present in one metallocene narrow molecular sample was absent in the chromium catalysed material. Banding and domaining were observed to dominate the overall crystalline morphology at the longest length scales, dominant lamellar structures at intermediate length scales and subsidiary in-filling lamellar structures at the smallest scale. These different divisions within lamellar texture were highlighted using a combination of electron microscopic techniques following permanganic etching.

Keywords: Crystallisation; Melting; Metallocene

1. Introduction

The need to produce semicrystalline polymers with chemically tailored molecular architectures, leading to greater control over processing characteristics and improvement of physical properties, has driven the chemicals industry since the early 1990s to manufacture a new generation of polyolefins synthesised with metallocene catalysts. The use of metallocene and single site catalyst technology has allowed the very rapid development of new olefin copolymers with a broad spectrum of structure and related physical properties. This technology is making significant inroads into commodity polyolefin markets. A gamut of metallocene/single site catalyst based olefin copolymers, including polyolefin elastomers, polyolefin plastomers, EPDMs, polypropylenes, polystyrenes and ethylene/styrene interpolymers (ESI) have been commercialised or are under final stages of commercial development. In addition to these areas of exploitation, exploratory work into other single site catalyst technologies that allow the copolymerisation of alpha olefins with polar comonomers is currently the focus of intense industrial and academic interest [1].

The main features that distinguish metallocene catalysts from all other catalyst systems are that they can: (a) polymerise almost any vinyl monomer irrespective of its molecular weight or steric hindrance; (b) produce extremely uniform polymers and copolymers of narrow molecular weight distribution and narrow compositional distribution; (c) control vinyl unsaturation in the polymers; (d) polymerise α-olefins with very high stereoregularity affording isotactic and syndiotactic polymers [2–5].

However, for our purpose, metallocene catalysed polyethylenes differ principally in the distribution of short chain branches (SCB) along the chain as shown by temperature rising elution fractionation (TREF) [6,7]. Whereas chromium catalysed polyethylenes have these placed at

* Corresponding author.
[1] Corresponding author.

0032-3861/00/$ - see front matter
PII: S0032-3861(99)00632-1

irregular intervals, metallocene polyethylenes have shown a tight, homogeneous distribution of SCBs with little or no long unbranched sequences [8–10]. In addition, a much narrower molecular weight distribution is usually produced. This distinction has been confirmed by Parker et al. [11] from high-pressure crystallisation, at 0.5 GPa, which produced crystal thickness distributions corresponding to the inter-branch separations. Independent small-angle X-ray scattering experiments allied with isothermal crystallisation and melting data have largely reaffirmed this observation [12,13].

The internal microstructure or morphology of semicrystalline polymers is central to their properties. The physical properties of semicrystalline polymers are largely dominated by constraints imposed through the extensive fold surfaces of their constituent lamellae and the presence of inter-lamellae tie molecules [14]. Different lamellar habits of defined lamellar thickness are conferred by crystallisation. However, they are inherently metastable with respect to crystal thickness, because of the greater reduction in fold surface per unit mass that occurs on thickening.

The kinetic theory of lamellar crystallisation from polymeric melts has had many successes but in recent times it has come under heavy criticism for its failure to describe accurately the observed temperature dependence of crystal growth rate in melt crystallised poly(*p*-phenylene sulphide) [15]. Despite these shortcomings, it is a theory that is based on the fact, that the rate-controlling step is secondary nucleation at a developing lamellar edge. In the early 1960s, Hoffman and Weeks proposed that the large elevation of melting point (T_m) above the crystallisation temperature (T_c) required lamellae to have thickened isothermally during growth by a factor γ [16]. The Hoffman–Weeks equation relates melting temperature to crystallisation temperature in the following way:

$$T_m = T_c/\gamma + T_m^0 - T_m^0/\gamma$$

where T_m^0 is the equilibrium melting temperature of an infinitely large crystal, free from defects, and γ is the thickening coefficient. Since their original proposal there has been no explanation of how the observed thickness of lamellae relates to that of the secondary nucleus, beyond their being linearly related by a constant factor γ of order three for linear polyethylenes [17]. This is the phenomenon of isothermal lamellar thickening. This process works because thin polymer lamellae transform to thicker and more stable ones when heated. Interestingly, in metallocene catalysed polyethylenes, γ is significantly larger [13,18]. At the same time, effective enlargement of the fold surface regions by the presence of excluded butyl branches is likely to occur. The preferential exclusion of branches greatly increases the potential gain of free energy on ordering by lowering the drive to lamellar thickening.

We have previously reported on lamellar systems, with limited thickening capacity based on calorimetry measurements [18]. These initial experiments on metallocene catalysed polyethylenes demonstrated that crystallisation occurs at least to within 3–4°C of their melting temperature, hence lamellar thicknesses will be approximately that of the (unthickened) secondary nucleus when $T_m = T_c$. This result leads to a direct method for determining the size of the original crystal nucleus. Recent experiments by Sutton et al. [19] on *n*-alkanes have reported chain extended crystallisation in a series of mono-dispersed paraffins, which has been interpreted by Hoffman as showing the critical nucleus to be as little as half the extended chain length despite T_m being very close to T_c [20].

Crystallisation of metallocene catalysed polyethylenes at constant thickness is conceptually different from linear chromium catalysed polyethylene in that the exploration of different chain conformations and folding intervals presumed to occur for the latter are denied in the former. In view of this, it is worth noting that when a branched polymer molecule adopts its final thickness, the system may pass through transient high energy branch-included conformations, somewhat analogous to the transient non-integral folding displayed by *n*-paraffin and low molar mass hydroxyl terminated polyethylene-oxide fractions [21,22].

In this paper, it is shown that by combining modulated temperature differential scanning calorimetry (MT-DSC) with electron microscopy (via permanganic etching), examination of morphology, crystallisation and melt-reorganisational behaviour in various medium density metallocene catalysed polyethylenes is possible. The crystallisation behaviour of metallocene polyethylenes as assessed through Avrami analysis is ranked against similar materials produced from conventional chromium processes. Apparent correlations in melt morphology between metallocenes of broad distributed molecular weights and conventional chromium catalysed polyethylenes exist in spite of the different catalyst types. This correlation among materials of broad molecular weight distributions from different catalyst types is absent in the case of narrowly distributed molecular weight metallocene catalysed polyethylenes [18].

2. Experimental and materials

2.1. DSC

All measurements were performed on TA Instruments 2920 DSC equipped with liquid nitrogen assisted cooling. This instrument was operated as a conventional heat flux DSC and as a modulated temperature DSC (MT-DSC). Temperature calibrations were made using high purity standards; benzoic acid, indium, tin, lead and zinc at a scan rate of 10°C/min. Calibration for heat flow scales was done using indium as reference and checked via heat capacity measurements with a sapphire disc in the range of interest. Temperature correction on cooling was performed

Table 1
Molecular and melting characteristics of as received material. Short chain branch content was assessed using ^{13}C NMR

Reference Catalyst type	Units	Polymer A Cr[a]	Polymer B Met[b]	Polymer C Met[b]
Density	g/cm^3	0.934	0.922	0.927
M_n	kDa	17	25.8	37.9
M_w	kDa	223	172	83
M_z	kDa	2303	734	147
M_w/M_n		13.2	6.7	2.2
SCB(/1000°C)[c]		6.8	9.7	4.3
T_m	°C	123.3	116.1	122.4
ΔH_m (10°C/min)	J/g	128.4	123.9	139.0
ω[d]	%	44	42	47

[a] Chromium catalyst.
[b] Metallocene catalyst.
[c] Butyl branches per 1000 carbon atoms.
[d] Weight fraction crystallinity.

using indium of various masses at different cooling rates and extrapolated to zero scan rates. Sample masses and reference pans were determined to the nearest microgram. An Intel Pentium 166 PC was used to collect and analyse the DSC thermograms.

Our ethylene/1-hexene random copolymers with known branch content, molecular weight and polydispersity were kindly provided by Fina Research (Belgium) through the Fina Surrey Scholar research programme. Details of as received materials are listed in Table 1.

2.2. Isothermal crystallisation kinetics

Isothermal crystallisation kinetic experiments were performed using two DSC instruments. TA Instruments 2910 DSC was used to heat specimens to 80°C above their observed melting temperature at a scan rate of 10°C/min where they remained for a period of 3 min under strong nitrogen purge. They were then transferred immediately in air to a 2920 MDSC, which was held at an isothermal temperature (in the range 90–123°C). During this transfer the temperature of the sample pan decreased by several degrees. The temperature of the pan was still well above the crystallisation temperature range and the highest measured melting point; equilibrium was established in the 2920 DSC within 20 s.

A second crystallisation procedure involved cooling specimens from the melt at 200°C in the 2920 DSC to a temperature just above the observed maximum melting temperature. This was followed by quenching to the desired crystallisation temperature (close-quench-temperature). This latter technique was frequently used to avoid undercooling effects commonly observed in traditional thermal programs. In both cases, the resulting crystallisation exotherm was recorded.

Examination of the melting process was investigated using conventional and MT-DSC. In conventional DSC, the preferred heating rate was 10°C/min. In MT-DSC, the preferred modulated conditions were heating rate 1°C/min, temperature modulation amplitude of 0.159°C for a 60 s period. The reversing and non-reversing heat flow signals were recorded and comparisons with the total heat flow signal from conventional DSC reported.

2.3. Determination of crystallinity

Crystallinity measurements were performed by integrating the overall melt and/or recrystallisation transition region and heat flow scales were normalised for sample mass difference. The literature standard for polyethylene, 293 J/g was used to represent 100% degree of crystallinity [17]. Crystallinity measurements were based solely upon heat flow and not heat capacity measurements because changes in heat capacity are known to take place well below room temperature, which would have affected our present set of results. We will consider heat capacity changes in a later publication.

2.4. Specimen preparation for electron microscopy

To prepare specimens for electron microscopy, compression moulded sheets were pressed at 140 kN pressure for 10 min at 175°C and subsequently cooled at 15°C/min down to room temperature [23]. Samples were then microtomed at room temperature using a rotary microtome removing successive slices of approximately 5 μm in thickness. An optical microscope with interference contrast was used periodically to assess the progress of microtoming. Specimens were etched for 3 h in an etchant consisting of a 1% (w/v) solution of potassium permanganate dissolved in 2:1 sulphuric and dry ortho-phosphoric acids [24]. Periodic checks on the progress of etching were undertaken, by arresting the etching process and observing development with the optical microscope. For TEM work, a standard two-stage indirect carbon replica was made of the etched specimen (using cellulose acetate film moistened with acetone). These replicas, which were several tens of nanometers in thickness, were then transferred to copper grids for examination in the transmission electron microscope.

2.5. Transmission electron microscopy

A Philips 400T electron microscope with EDS capability was used to examine carbon replicas in bright field mode under an accelerating voltage of 80 kV. Specimens were mounted in a rotating goniometer stage capable of *xy* movement in the plane of the specimen as well as in/out-of-plane tilt. Tilting of replicas with respect to the electron beam was used occasionally to enhance resolution and to obtain clarity of complicated microstructural details.

2.6. Gel permeation chromatography

A WATERS 150-CV GPC was used to determine

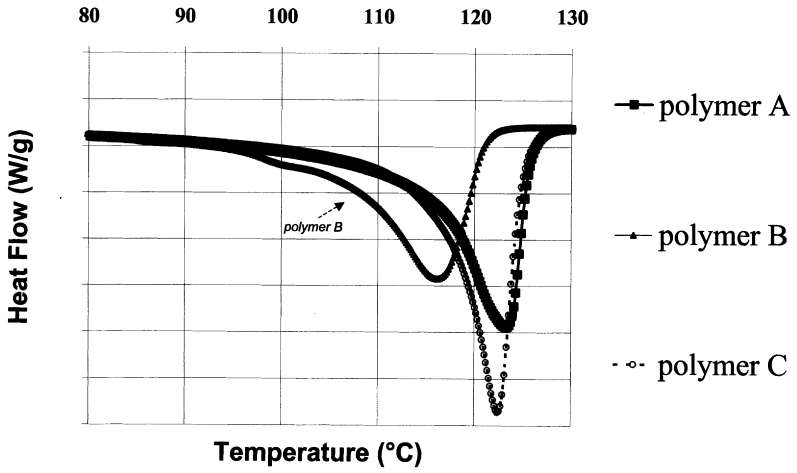

Fig. 1. A series of melting endotherms of as received medium density polyethylene pellets.

molecular weight characteristics of our materials. Standard procedures were adopted using dichlorobenzene as the solvent, which was distilled before use. The 150-CV incorporates a size exclusion chromatography (SEC) dual detection system (both refractive index and viscometric detectors); this allows the possibility of absolute molecular weight determination using universal calibration. Fractionated polyethylenes and polystyrene standards were used as calibrants and polystyrene standards were also run as unknowns to verify the calibration plots.

3. Results

3.1. Thermal characterisation

Fig. 1 shows comparative melting traces of as received chromium versus metallocene catalysed medium density polyethylenes. The molecular characteristics and initial thermal properties of these polymers are tabulated in Table 1. In analysing the melting curves, we elected to integrate the melt region from a point where the underlying baseline started to deviate from its room temperature value to its return 20°C above the main melting transition [18].

3.2. Kinetic melting

Fig. 2 highlights results obtained from MT-DSC experiments for one metallocene-catalysed polyethylene (polymer B). MT-DSC is a relatively recent invention by Reading [25] and its use in studying semicrystalline polymer melting behaviour is still in its infancy. One of the important advantages of this technique over conventional DSC is that of enhanced resolution without loss of sensitivity and the separation of reversing and non-reversing thermal transitions (e.g. a reversing glass transition from a non-reversing curve exotherm). MT-DSC contains the same heat flux arrangement, but a different heating profile that consists of a sinusoidal temperature modulation overlaid on a traditional linear heating ramp. Deconvolution of the signals in MT-DSC separates the "total" heat flow into its heat capacity related (reversing) and kinetic (non-reversing) components. We used the standard deconvolution methods available on the TA Instruments 2920.

Fig. 2(a) shows the MT-DSC non-reversing heat flow signal, the reversing heat flow signal and the total heat flow signal of a sample of polymer B crystallised at an isothermal crystallisation temperature of 90°C for 1 h, cooled to ambient temperatures and re-heated. Exothermic behaviour associated with structural reorganisational activity was observed in the non-reversing heat flow signal and appeared absent in the reversing heat flow signal.

Fig. 2(b) shows the MT-DSC response for polymer B crystallised at 115°C. In this case the total heat flow and the reversing heat flow signals show clear evidence of two well separated melting transitions. In contrast to Fig. 2(a), the non-reversing heat flow signal in Fig. 2(b) contains a reorganisational exotherm coincident with the lower temperature melting transition. In addition, an exothermic transition is coincident, but out-of-phase with the higher temperature melting transition. The significance of this is at present unclear but we believe it may be associated with kinetic overshoot effects, which are currently being investigated.

3.3. Crystallisation kinetics

Fig. 3 shows the evolution of typical crystallisation exotherms for polymers A, B and C over the widest isothermal crystallisation range possible. In all three cases, a high temperature conditioning cycle at 200°C in the melt preceded the crystallisation procedure. This particular step ensured that existing crystal-nuclei and melt history were removed. In all three examples, the average degree of pseudo-undercooling was approximately 7°C below their respective peak melting temperatures. In these examples

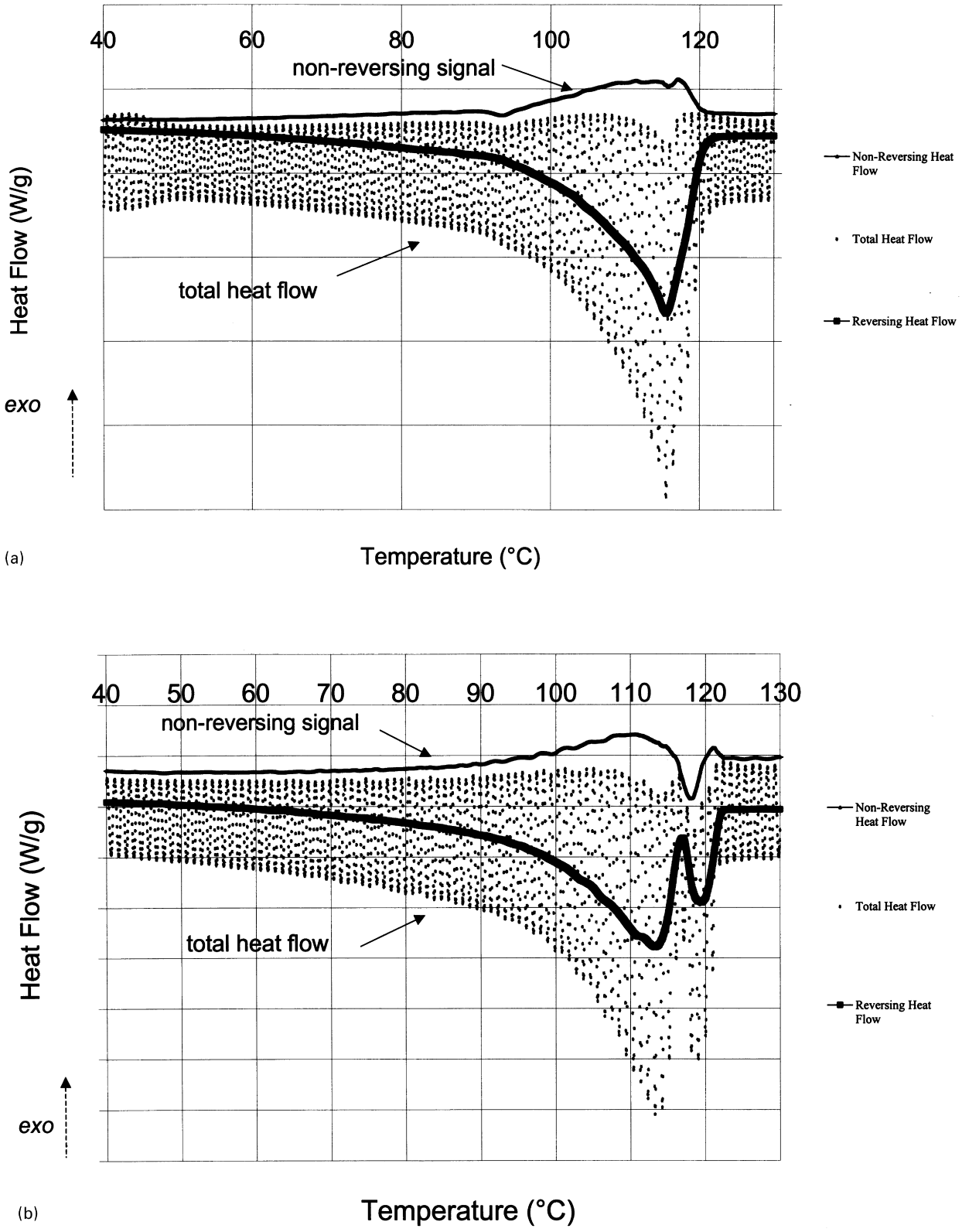

Fig. 2. Modulated temperature DSC traces on heating of polymer B crystallised at 90 and 115°C for 1 h following slow cooling (approximately 1°C/min) down to room temperature. Modulation conditions were: 0.159°C amplitude, 60 s period and an average underlying heating rate of 1°C/min. (a) represents the heating trace of a specimen crystallised at 90°C. The top curve shows the non-reversing heat flow signal (b) which represents a specimen crystallised at 115°C. The top curve shows the non-reversing heat flow signal.

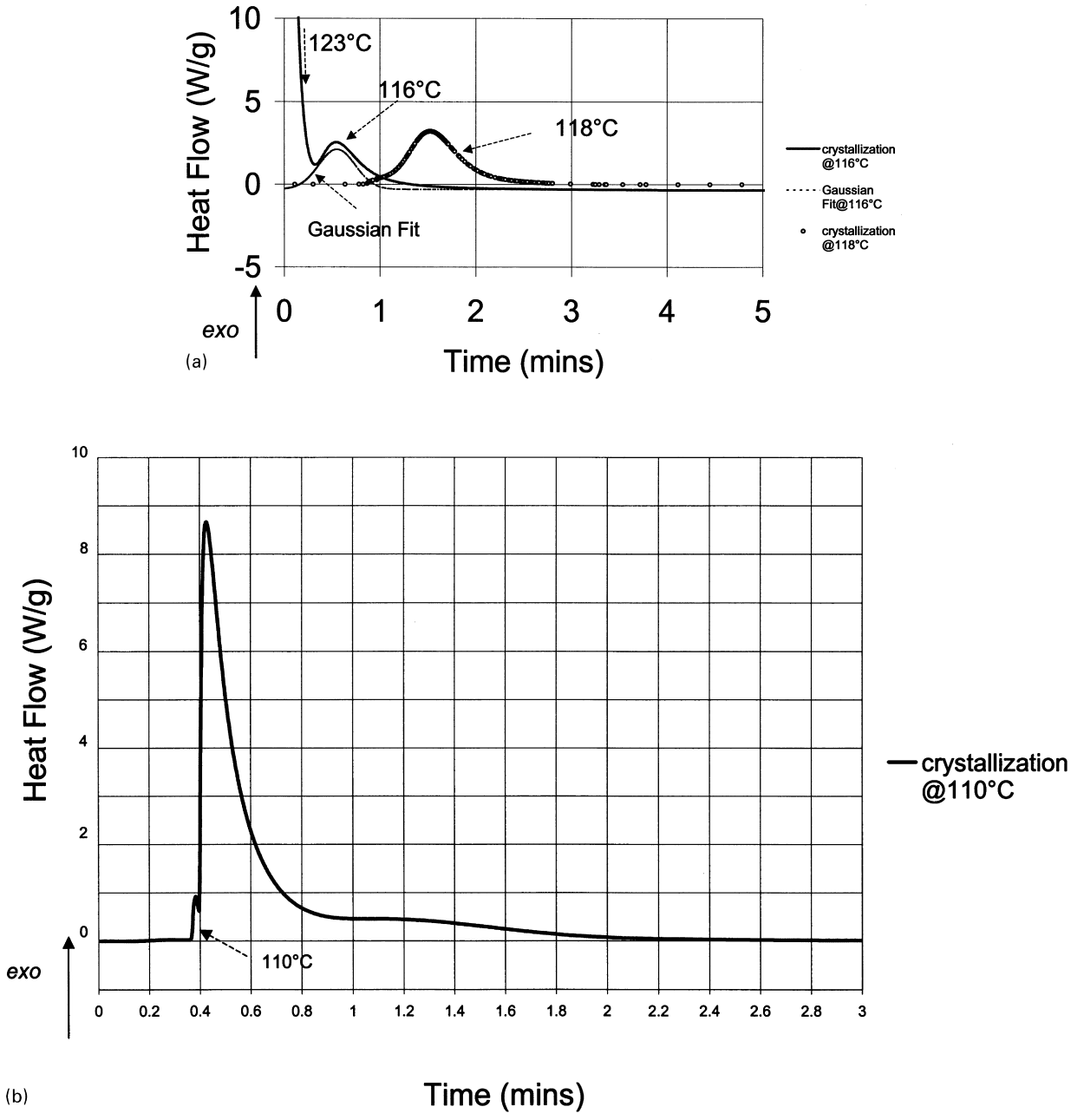

Fig. 3. (a) Crystallisation exotherm of polymer A at 116°C $t_{0.5}$ occurs after 30 s crystallisation and complete crystallisation was attained after 5 min. The measured heat of fusion was 21 J/g, estimates using a Gaussian deconvolution peak fitting algorithm (dashed line) puts this at twice the value, i.e. 40 J/g. Also represented is the isothermal crystallisation exotherm at 118°C, $t_{0.5}$ that occurs after 90 s. (b) Crystallisation exotherm of polymer B at 110°C $t_{0.5}$ occurs after 40 s crystallisation and complete crystallisation was attained after 10 min. The heat of fusion was estimated at 60 J/g corresponding to approximately 20% crystallinity. (c) Crystallisation exotherm of polymer C at 114°C Local minima in growth rate found after 60 s crystallisation with complete crystallisation occurring shortly thereafter. The heat of fusion was estimated at 68 J/g corresponding to approximately 23% crystallinity.

the isothermal crystallisation procedure involved cooling samples from just above their observed melting temperature of 125°C to the crystallisation temperature of 116°C for polymer A, from 118 to 110°C and from 125 to 114°C for polymers B and C, respectively.

Fig. 3(a) shows the crystallisation exotherm of polymer A crystallised under both pseudo isothermal (116°C) and isothermal conditions (118°C). The crystallisation exotherm at 116°C is superimposed on the reducing heat flow curve associated with the DSC achieving thermal equilibrium on changing the isothermal temperature from 123 to 116°C. The deconvoluted crystallisation exotherm is fitted best by a Gaussian curve as shown in Fig. 3(a). The maximum in crystallisation rate was achieved after only 30 s compared with 90 s at 118°C. The 118°C exotherm is unaffected by equilibration effects. The degree of crystallinity at 116°C

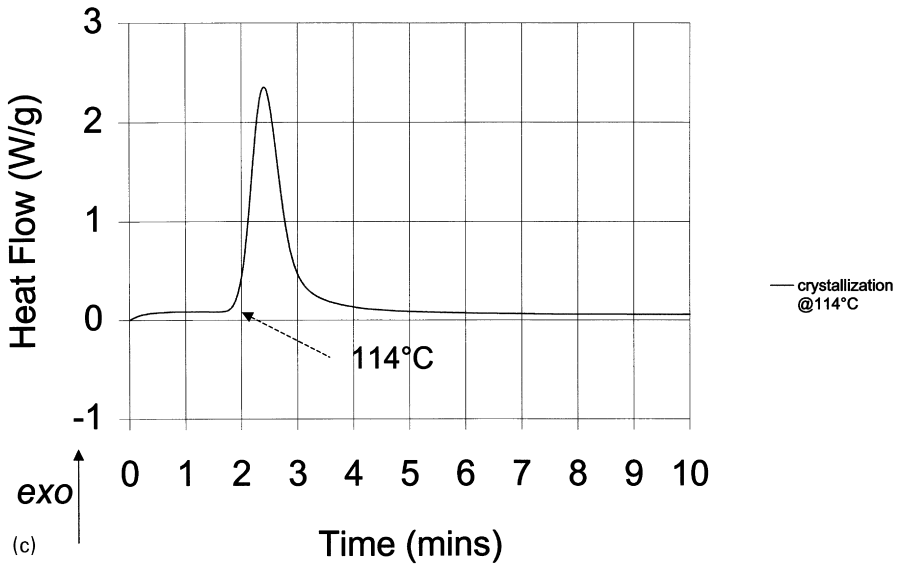

Fig. 3. (*continued*)

estimated from an approximate integration of the area under the curve was 10%. Subsequent melting without cooling put this value as being just one-half the total crystallinity achievable at this temperature. Integration of the crystallisation exotherm at 118°C produced a weight average crystallinity of 20%, which was a little lower than the measured crystallinity on re-melting.

Fig. 3(b) and (c) shows isothermal crystallisation exotherms for polymers B and C at 110 and 114°C, respectively. In Fig. 3(b), the peak in the curve occurs approximately 40 s after attaining quasi-equilibrium conditions (total heat flow equal to zero) with all primary crystallisation processes complete after 2 min with further rearrangements occurring out to 3 min. In this example, a clear shoulder is observed in the crystallisation curve at times greater than one minute. Small exothermic fluctuations appear to the right of the main peak which are related to small temperature variations following the main crystallisation process. The total crystallinity was measured from the integral of the complete exothermic curve and found to be 20%. This value compares closely with the heat of fusion value obtained on immediately heating and re-melting the sample; the degree of crystallinity was found to be 20%. For polymer C, Fig. 3(c), the crystallisation behaviour is similar to that of polymer B with only one main crystallisation exotherm with a maximum occurring 140 s after the onset of crystallisation. A small delay prior to crystallisation that may be related to an induction period was observed in Fig. 3(c). In this example, crystallisation is largely complete within 5 min and the measured crystallinity of approximately 23% was also confirmed by the heat of fusion value on re-melting.

3.4. Avrami analysis

In describing the overall crystallisation kinetics, Avrami analysis was applied to quantify crystallisation rate constants and define the types of crystallite geometries generated by crystallisation [26,27]. For our materials, the weight fraction crystal transformed on isothermal crystallisation was obtained through discrete partial integration of the area under the melting/crystallisation curve normalised by the total area under the curve. The Avrami expression can be written in its most familiar form of

$$\Delta H_f(t)/\Delta H_f(\text{tot}) = 1 - \exp(-kt^n)$$

where $\Delta H_f(t)$ is the change in heat evolution at time t and $\Delta H_f(\text{tot})$ is the total heat evolved for complete crystallisation. $\Delta H_f(t)/\Delta H_f(\text{tot})$ is a measure of actual crystal transformation, k is the rate constant, t, the time of crystallisation and n, the Avrami exponent.

The Avrami analysis of polymers A, B, and C at the same average "relative" undercooling of 7°C is shown represented in Fig. 4. The degree of relative undercooling, ΔT is estimated as $T_m(\text{observed}) - T_c$. For polymer A, $\Delta T =$ 7°C, polymer B, $\Delta T = 6$°C and for polymer C, $\Delta T = 8$°C. Fig. 4 shows the analysis following standard Avrami treatment of polymer A crystallised at 116°C, polymer B crystallised at 110°C and polymer C crystallised isothermally at 114°C.

In the case of polymer A only one structural development process can be described from the straight line fit to the data. The total crystallizable fraction was estimated to be 14% at this temperature corresponding to $\Delta H_f(\text{tot}) = 40$ J/g. The equation which best describes the linear fit through the data series was $y = 1.5x - 1.9$.

In the case of polymer B crystallised isothermally at 110°C two different structural development processes are seen taking place. The first which ends after approximately 40 s crystallisation is immediately followed by a second process that takes place over a longer period of time. The

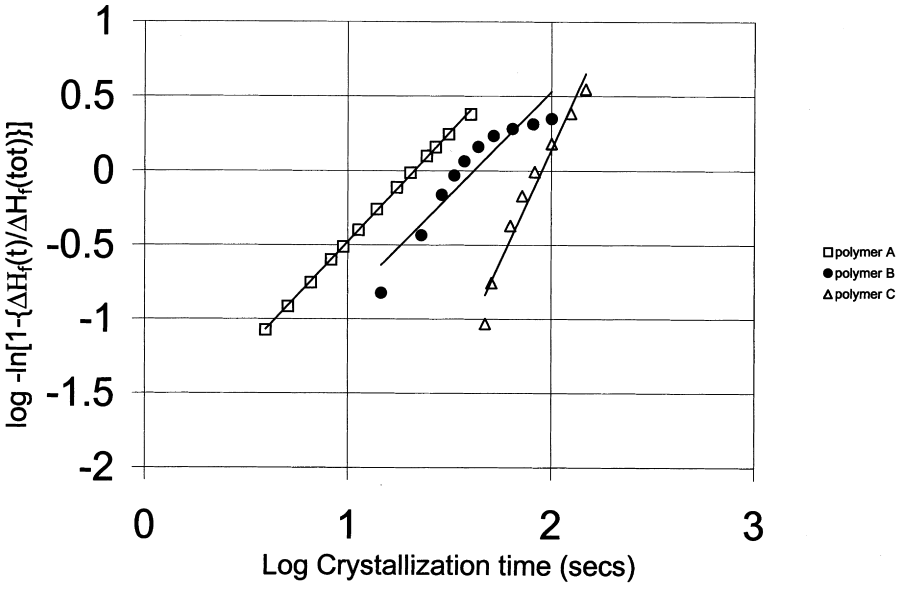

Fig. 4. A plot of log − ln[1 − {$\Delta H_f(m)/\Delta H_f(\text{tot})$}] versus logarithm of crystallisation time (min) taken from Fig. 3 for polymer A at 116°C, polymer B at 110°C and polymer C at 114°C represented in classical Avrami format. The straight lines through the data set represents the best lines of fit using the method of least squares.

total crystallizable fraction was 22% at this temperature corresponding to $\Delta H_f(\text{tot}) = 63$ J/g. A least squares fit was drawn for this set of data and the equation which describes best both initial and later processes is $y = 1.4x - 2.3$.

In the case of polymer C crystallised isothermally at 114°C only one structural development process is evident despite the small amount of dispersion in the data. The total crystallisable fraction was 23% at this temperature corresponding to $\Delta H_f(\text{tot}) = 68$ J/g. A least squares fit was drawn through both the initial and later processes and the equation of best fit was calculated as $y = 3.0x - 5.9$.

3.5. Transmission electron microscopy

Fig. 5(a) shows a low magnification electron micrograph of chromium catalysed polymer A following crystallisation at a cooling rate of 15°C/min from the melt. The gross texture is one of partially ordered domains of lamellae. The arrows indicate a typical domain. Lamellar domaining is seen throughout and is heterogeneous within the specimen. Domain size varied considerably from 0.1 to 2 μm, which probably scales with nucleation centre spacing. In these domains, the average lamellar thickness was approximately 20 nm. The domains could be described as irregular crystal aggregates or immature spherulites. No particular orientation could be identified because their overall form adopted a mosaic-pattern texture.

There are however, three distinct levels of texture, which are distinguishable in this material. Fig. 5(b) shows a high magnification view of the domain area already highlighted in Fig. 5(a). Of the three textured levels, the mosaic form is by far the largest, i.e. groups or aggregates of locally oriented lamellae forming a mosaic structure, which occupies a single domain. Detailed observations of the crystal aggregates reveals a second dominant level of crystalline texture, namely primary lamellae forming basic growth units. Examples have been labelled A (top right-hand corner indicated by arrows). These basic units appear as stacks of different profiled lamellae varying in shape from curved to planar. At the third level, small fine-textured planar lamellae, labelled B, are slightly thinner and shorter. Historically, this latter type of lamellar texture has been described in the literature as in-filling with lamellar growth trajectories developing along classical lines. In this figure what we observe is unprecedented, in-filling lamellae develop by growing at a high-subtended angle (almost perpendicular in some cases) to the dominant lamellar species. In Fig. 5(b) we also see evidence of hampered planar domains located at inter-domain boundaries in the plane of the micrograph.

An interesting feature of the etching process is its capacity to selectively digest areas of lower crystalline density. In the region, labelled C curved dominant lamellae that have been etched to varying depths are revealed. Edge-on lamellae are seen circularly in this particular area in the sample where several layers of lamellar structure are exposed from the underlying surface. The morphology of this specimen embraces textural aspects common to both high density and linear low-density polyethylenes. The net result is a varied composition of lamellar textures that represent medium density polyethylene microstructure.

Fig. 6(a) shows a low magnification view of the melt-crystallised morphology of the first metallocene material, polymer B. Lamellar textures similar to those in polymer

Fig. 5. TEM carbon replica of polymer A viewed at: (a) low magnification showing lamellar domaining, ranging from 0.1 to 2 μm; (b) high magnification showing several textured lamellar forms and lamellar thicknesses ranging from 10 to 20 nm.

A are seen here. The salient textural features of this morphology are lamella domains and intermediate substructure. Lamellar domains are seen at approximately 0.5–1 μm in size and well separated from each other. Label D highlights planar profiled lamellae with some degree of dominant/subsidiary lamellar structures in which the subsidiary lamellae subtend a high acute angle to the dominant group. The observed lamellar thickness is not so

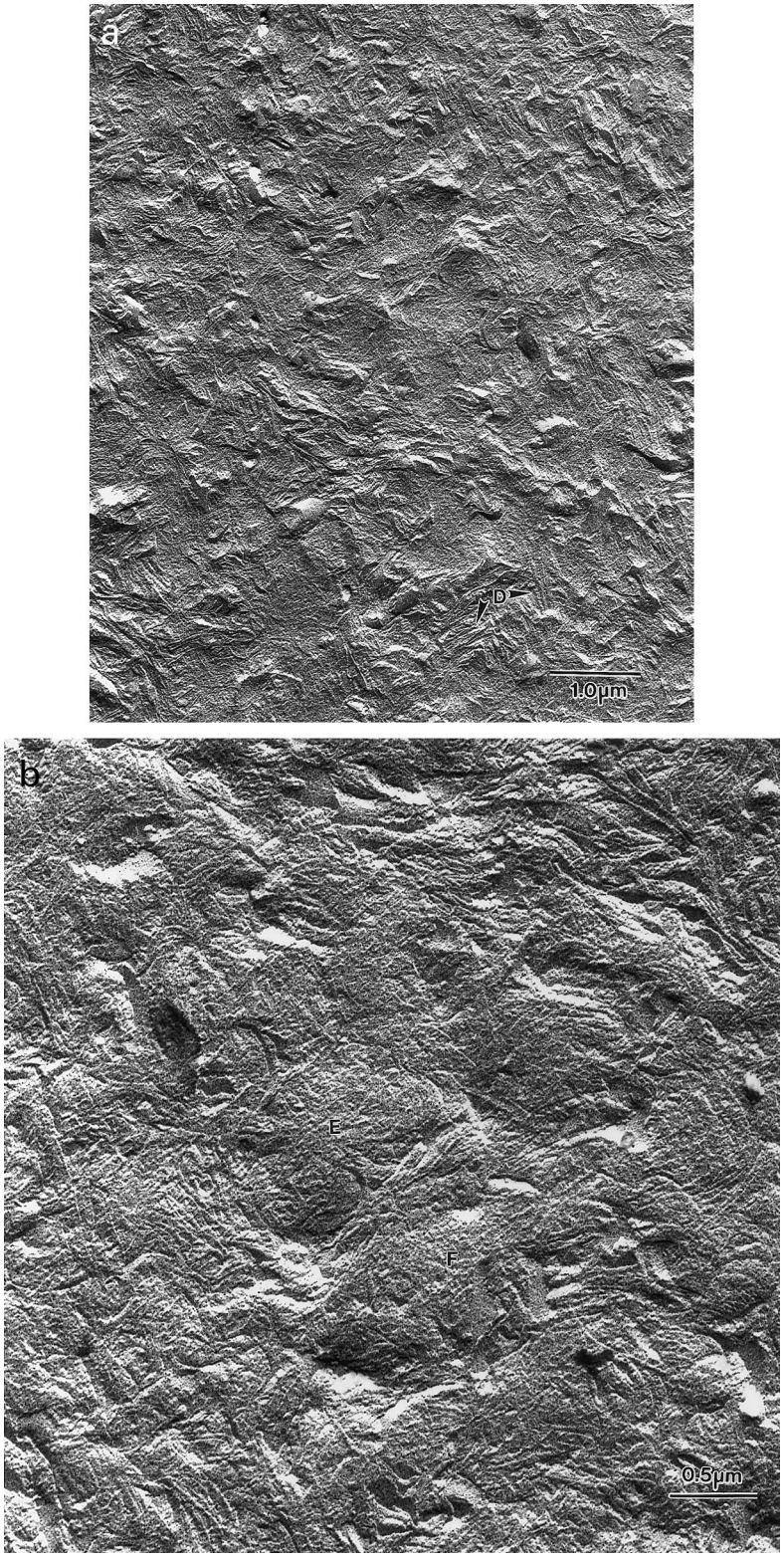

Fig. 6. TEM carbon replica of polymer B viewed at: (a) low magnification; (b) high magnification. Lamella domains occur at approximately 0.5–1 μm in diameter intervals standing proud from the underlying fine grain morphology.

widely distributed as in the case of polymer A having an average value of 17 nm. In addition, the partitioning of the three types of crystal architecture seen in polymer A is more diffuse. Fig. 6(b) shows a close up view of both large-scale morphology and fine scale (in-filling) lamellar detail. In the centre of the image, two lamellar domains of approximately 1 to 2 μm in diameter, labelled E and F, respectively, act to sandwich a sheaf of edge-on planar lamellae.

Fig. 7(a) shows the second metallocene material, polymer C, at low magnification. In this case, the sample shows several banded spherulites, which have undergone impingement. The region in-between these impinged structures are of the order of several micrometers in diameter. Close examination of these banded structures show significant departure from circular symmetry. In this view, the spherulite is exposed in a near-central view but sufficiently off-axis to create a departure from circular symmetry of the bands. Off-centre cross-sections would have a smaller number of circular bands visible and a significantly higher population of S-profiled lamellae. Generally, in predominately off-centre cross-sections, S-profiled lamellae would be seen between spherulites and at the inter-spherulitic boundaries. In all cases inter-spherulitic boundaries feature a dramatic change in crystal orientation, highlighted in Fig. 7(a), and again at a higher magnification in Fig. 7(b) by a set of arrows. In Fig. 7(b) a clear boundary layer is observed which is approximately the size of the observed band spacing.

On closer examination, polymer C contains coarse spherulitic structures interspersed with dominant lamellar textures with in-filling subsidiary lamellae buried within them. Fig. 7(b) and (c) highlights these observations. Flat-on lamellae are seen clearly in Fig. 7(b) standing proud of those which are edge-on (which gives alternating relief to banded spherulites). This relief occurs as a result of etching efficiency being higher edge-on than on the fold surface of lamellae; this results in flat-on basal surfaces always standing higher than edge-on lamellae. Equally, band periodicity is uniform and regular with evidence for in-filling lamellae (dominant/subsidiary structures). In-filling is best observed when flat-on lamellae are radial to the crystallographic *b*-axis and overlapping lamellae are splayed apart at large angles. This occurs predominantly when the centre of a spherulite is well above or below the radial plane, and lamellae are growing out of the plane of the picture. All lamellae are then seen edge-on. This position is particularly useful for observing S-profile regions where short in-filling lamellae are also seen between S-shaped crystals.

At a still higher magnification, Fig. 7(c) shows both S-profiled and in-filling lamellar structures. In-filling between adjacent dominants usually involves three or four planar profiled lamellae in close proximity (25 nm or closer). Arrows highlight an area where this is clearly visible. Lamellar thicknesses in this sample were comparatively lower than the other two materials with values estimated at around 15 nm.

The issue of banding and its causes arise because, although the *b*-axis remains steady as outward growth occurs, the *a* and *c*-axes appear to spiral continuously about the growth direction. Each turn of the planar lamella through 180° produces a band spacing which in the case of polymer C is about 0.8 μm.

4. Discussion

From Table 1 it is clear that our three polymers have similar crystallinities despite clear differences in short chain branch content, polydispersity and melting temperature. These differences relate to the different catalyst systems used for polymerisation. Comparisons between the various polymers show that with the exception of polymer B the other polymers have a narrow melting range. In fact, polymer A despite having the higher polydispersity has the highest melting temperature.

From the MT-DSC results of Fig. 2(a) and (b), separation of a second melting endotherm in polymer B appears evident, while development of a dual melting peak in the reversing heat flow signal is seen most clearly at the highest crystallisation temperature of 115°C (Fig. 2(b)) with strong evidence for reorganisation processes occurring throughout the crystallisation range examined. In Fig. 2(b) a large upper melting temperature peak is observed in the reversing heat flow signal that is absent in Fig. 2(a). The common explanation offered in interpreting dual melting behaviour is based on molecular considerations. Typically, slow rates of crystallisation like those used in our experiments lead to greater molecular segregation resulting in more and less perfect crystals having different melting temperatures. Molecular segregation effects are much reduced at lower temperatures where crystallisation that is more rapid occurs and where segregation may occur on a much finer scale. Discerning these differences within a large ensemble of crystals is quite difficult when only one broad melting peak is displayed.

Crystallisation behaviour is a key differentiator in these materials. Crystallisation at an average relative undercooling of 7°C, shows that the chromium catalysed material of polymer A crystallises faster than metallocene catalysed polymers B and C in descending order. If we consider such comparisons only from the magnitude of the melting point, then polymer B crystallises most favourably followed by polymers A and C in descending order. Further differences can be seen in the Avrami plots particularly at higher isothermal crystallisation temperatures. The Avrami exponents increased with increasing crystallisation temperature and the rate constants show a corresponding increase. Polymer C with its higher Avrami exponent of 3, typical of spherulitic growth, is an exception among this group of polyethylenes. Lower Avrami exponents ($n = 1.8$–2.6) found for polymers A and B have also been observed in the literature [28]. In principle, one could determine the nucleation rate constants from a priori knowledge of the spherulitic growth rates, however this is problematic since most of our spherulites and domains are very small. All three polymers studied here exhibited the same early stages of crystal growth with rate constants ranging from a projected $2.2\ s^{-1}$ for polymer A to $2.8\ s^{-1}$ for polymer B. Relative to polymer A, polymer B also had a slightly larger degree of supercooling, which would explain its smaller rate

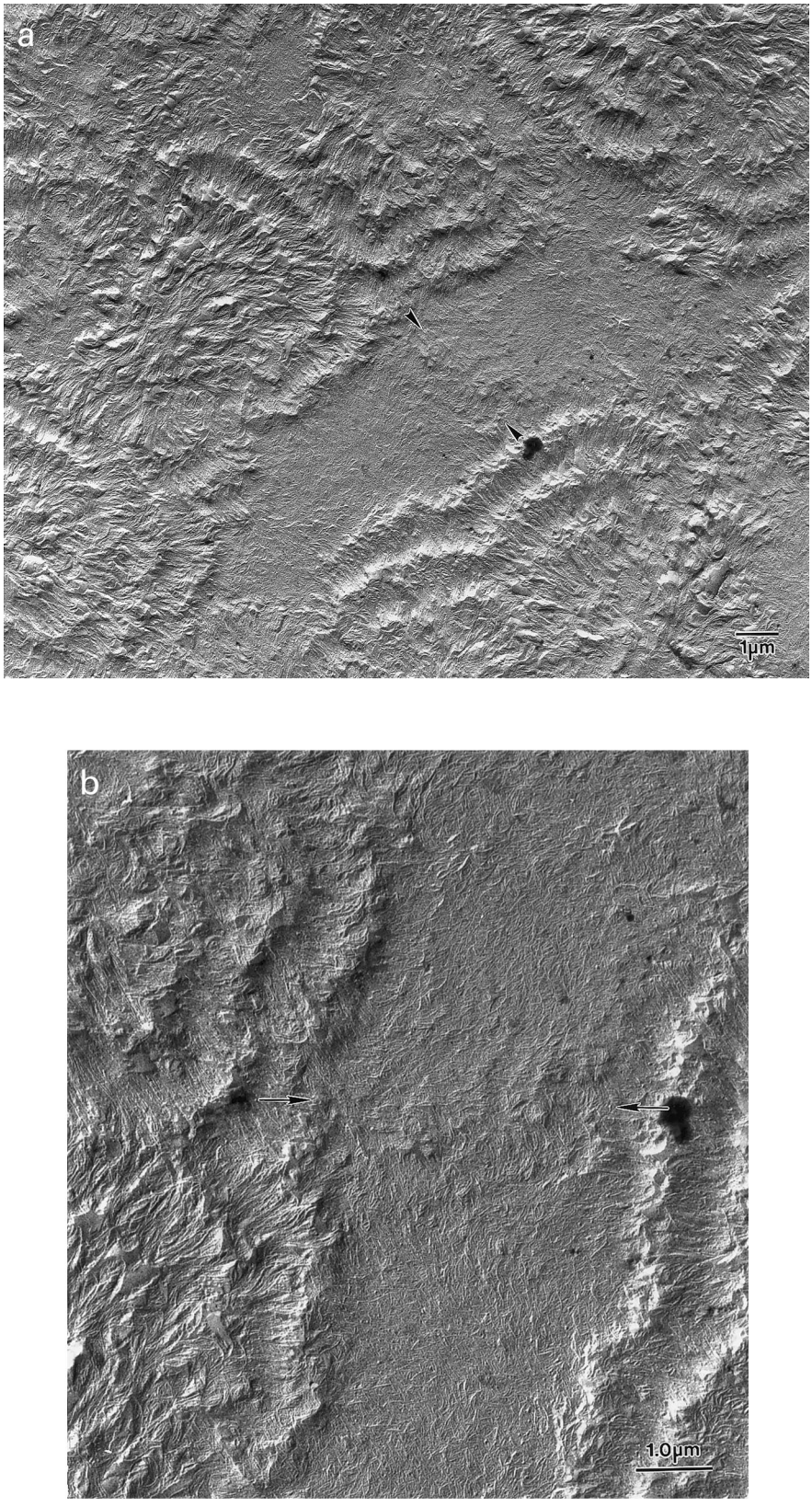

Fig. 7. TEM carbon replica of polymer C viewed at a near non-diametral section: (a) low magnification image with a band period of 0.8 μm; (b) close-up of interspherulitic regions revealing aspects of flat-on and edge-on lamellar structures inter-mixed with fine detailed sub-structure and in-filling lamellae; (c) high magnification of the polar region of a spherulite at maximum radius. S-profiled lamellae are seen exposed mainly in edge-on projections.

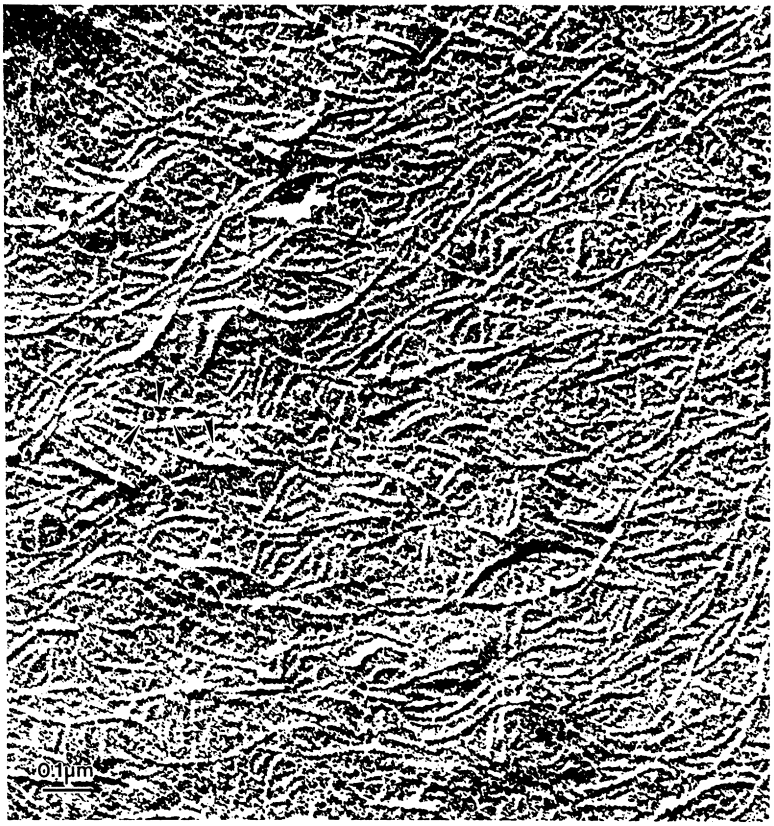

(c)

Fig. 7. (*continued*)

constant. Polymer C on the contrary, with the highest average undercooling had the lowest rate constant of $k \sim 1.7\ s^{-1}$. Commenting on the observed trends in the Avrami plots for polymers A, B and C, we have found an appreciable deviation from linearity at the latter stages of crystallisation, which is akin to the phenomenon of secondary crystallisation.

We suggest that the smooth transition from one crystal population to the next during crystallisation would probably correspond to the time for spherulitic or domain impingement. Initial exploratory polarised optical microscopy work suggests that this is likely to be the case. Further, we would anticipate that at impingement, there would be a change in the crystallisation kinetics marked by a significant difference in bulk crystallinity. Related studies on low molar mass polypropylene fractions have shown this to be the case [29]. This would seem to indicate that the secondary crystallisation process, associated with the lower Avrami exponent, proceeds on a finer textural scale in regions between the primary lamellae. In this case initial primary or dominant lamellae will stop growing at impingement and crystallisation will proceed in unoccupied regions between these lamellae which may account for our observations of subsidiary lamellae.

In spite of the obvious differences between polymers A and B, i.e. polymerisation using different catalyst types producing different molecular weight distributions and level of short chain branching, their overall microstructures were very similar when examined at low magnifications in the electron microscope. Essentially, the fine morphological textures of polymers A and B arise as a result of high nucleation that occurs on a sub-micron to micron length scale. In general, if the nucleation density is low enough, one can observe large banded spherulites with band periods several tens of microns in length as in polymer C. In polymers A and B the nucleation spacing is probably closer than one band period. We believe we may be seeing evidence for this. In this case, we observe crystal aggregates that take on the appearance of domains. In spherulitic systems, lower temperatures of crystallisation produce closer bands and one is more likely to see banding in rapidly cooled specimens. With high molecular weights, tighter bands are also observed but if the nucleation density increases more rapidly than the reduction in the band spacing then banding will not be observed [30]. This is probably most likely the case in our broadly distributed polymers since polymers B and A in particular show an appreciable high molecular weight component in the molecular weight component. Further, aspects related to molecular composition and chain heterogeneity are the subject of a forthcoming paper [31].

Typically, lamella profile is known to vary systematically with crystallisation temperature, time and molecular weight. The range of profiles identified for polyethylene lamellae are many, they range from "ridged" profiles at low molecular weights and high temperatures of growth, to curved lamellar profiles at lower temperatures. The transition from ridged/planar forms to curved, and eventually S-profile forms is more strongly dependent upon crystallisation temperature than any other independent variable for high molecular mass polyethylenes. At low crystallisation temperatures, S-shaped lamellae develop with a large pitch angle leading to a reduction in chain inclination. In our polymers, be it metallocene catalysed or chromium catalysed we have observed a mixed population of both curved and planar forms, indicating we believe that at isothermal crystallisation temperatures, molecular segregation and fractional crystallisation is an active process in determining the overall crystalline composite morphology [18]. We have observed an open array of primarily dominant S-shaped lamellae (high molecular weight component) with the defective material (branched low molecular weight) present as subsidiary lamellae in between. Crystallisation occurs primarily by selecting those chains with the longest branch free sequence, i.e. the "more linear" component. These distinct differences in lamellar profiles at a constant crystallisation temperature can also be interpreted in terms of molecular nucleation controlled growth processes. Recent findings from TEM on high density metallocene catalysed polyethylenes show that in-filling concentration and angular position with respect to leading dominant lamellae can be modulated by changing the crystallisation conditions [32].

Clearly, polymer molecules of finite length experience a broad range of equilibrium properties and thus different equilibrium melting temperatures. These differences lead in turn to different kinetic driving forces, at similar degrees of supercooling. The effect of supercooling and fractionation is seen clearly for branched, low molecular weight material, which will crystallise more slowly relative to high molecular weight less branched material at elevated crystallisation temperatures. Typically in chromium catalysed polyethylene copolymers fractionation occurs primarily based on branch content, and hence the length of branch free sequences rather than branch size. Correlations between melting and branch content following selective extraction experiments have shown that melting points can vary with branch content provided the branches are excluded from the crystal, namely, branches greater than methyl [33]. Recent work by Kim at al. [34] demonstrated that the branch length effect on melting point depression can be significant with long branches producing larger melting point depressions. In our compression moulded specimens we suspect that low molecular weight material crystallises later in between adjacent planar/curved dominant lamellae producing slightly thinner planar lamellae separated by at least 25 nm of an amorphous layer.

An important consideration when developing products with specific end use applications is one of designing chain characteristics to tailored-engineered physical properties. Interestingly, with the exception of polymer C, little difference in lamellar thickness was observed among the other two materials. We could infer that the molecules in curved stressed-free lamellae have the luxury of exploring different conformations prior to final registry in the crystal lattice. This possibility is not available a priori in the more planar profiles of low molar mass materials. Further, we could suppose that regular positioning of branches "pin-down" molecules in lamellae of high molecular weight preventing lamellar thickening from taking place. Polymer C, which represents our most chemically regular polyethylene, has a theoretical inter-branch separation of 24.2 nm (assuming a homogeneous distribution of branching). This value is approximately one and a half times the observed average value of 15 nm as measured directly from TEM.

Using the Gibbs–Thompson equation for melting point:

$$T_m = T_m^0(1 - 2\sigma_e/\Delta h_f l)$$

and substituting, $T_m^0 = 141.5°C$, $\sigma_e = 0.093\ J/m^2$ and $\Delta h_f = 3 \times 10^8\ J/m^3$, yields for a melting temperature (Polymer C) of 122°C, a value for l of 13.5 nm, i.e. broadly in line with lamellar thickness resolved by electron microscopy but about half the interbranch separation distance. This value is consistent with respect to the experimental observation of 15 nm. The apparent discrepancy in this experimental value and the theoretical inter-branch spacing of 24.2 nm can be rationalised on the grounds of a quasi-micellar lamellar model. In attempting to pictorially represent an appropriate lamellar profile, that represents schematically both experimental and calculated lamellar thicknesses, in Fig. 8 we have drawn two polymer chains labelled 1 and 2 undergoing chain folding with butyl branches excluded from the crystal fold surface. The average crystal core thickness of 15 nm highlighted by a dotted parallel array of lines is shown. We recognise that alternative models may also describe the results equally well.

In our broadly distributed metallocene polyethylenes the relative distribution in crystal thickness is too imprecise to establish clear relationships between the calculated inter-branch separation and the lamellar thickness. With polymer A in particular, there appears to be an upper thickness limit. This could correspond to a semi-ordered meshing of branches from adjacent layers in metallocenes with regular branch spacing and which is absent in chromium catalysed polyethylenes with more random branch spacing.

The molecular picture that is being described here can be envisaged to lead to pseudo planar lamellae with adjacent re-entry folding and quasi-positionally ordered arrays of branches (butyl branches in our polymers) with 0.5–1 branch per fold in the fold surface. Moreover, the array in the surface of one layer should be able to interdigitate with those of its neighbour (as shown in Fig. 8) to give a thin layer of butyl branches sandwiched between the two

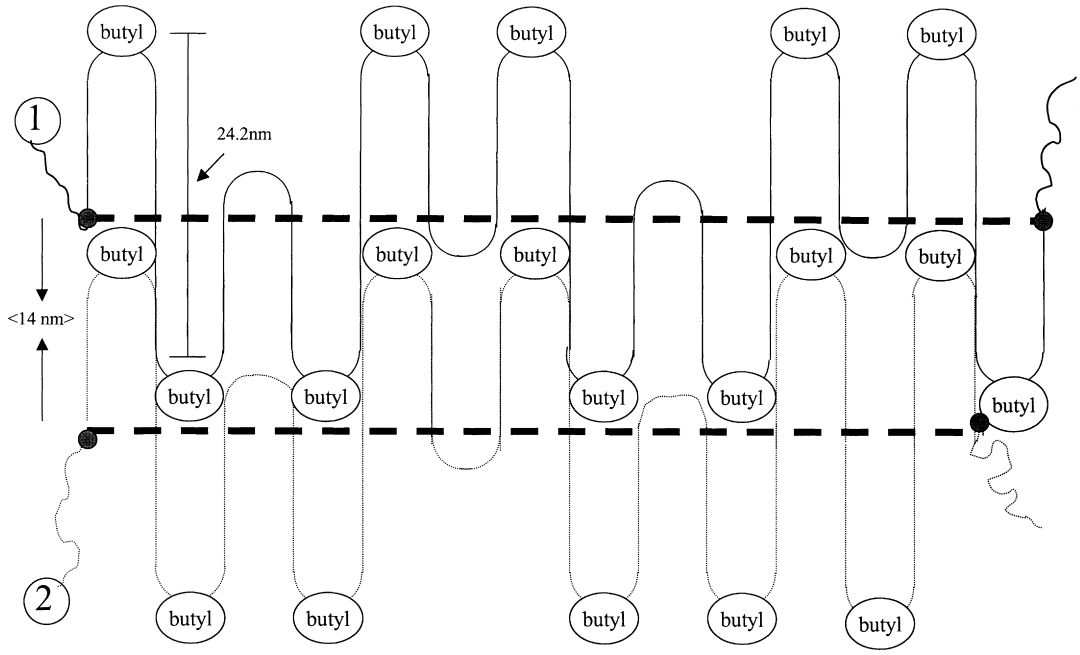

Fig. 8. Schematic representation of two polymer chains labelled 1 and 2 within a pseudo thin polymer lamella of polymer C with butyl branches at the fold surfaces meshed between each lamella. Each long segment incorporating one fold and one branch is met by subsequent segments of two folds and two branches. The calculated distance between any two branches is 24.2 nm whereas measured and observed values for lamellar thicknesses rest around 15 nm.

lamellae. This meshing of branches in the fold surface regions may have a strong effect on tie-molecule characteristics and mechanical properties, especially the great ductility shown by crystal mats of copolymers of polyethylene in contrast to the brittleness of similar linear materials [14].

Polymer C which has a high proportion of this more uniformly branched molecular architecture still manages to crystallise in spherulitic form. Typically, spherulites are built from an open lamella framework within which later-crystallising species are accommodated. For typical linear polyethylenes, it is the shorter molecules that solidify later; for copolymers, however, it is the more branched molecules. This difference no doubt imparts different susceptibilities to processes such as slow crack propagation [35] and environmental stress cracking [36]. In our metallocenes, we anticipate that shorter molecules will crystallise later. However, we have seen in this study and in previous works what appears to be a degree of fractional crystallisation, both at high and low growth temperatures in particular for broadly distributed molecular weight polyethylenes, which, effectively are blends with linear polyethylenes [18]. Recently, Cheng et al. have compared Ziegler–Natta copolymers with single site metallocene catalysed polyethylenes with different loadings of short chain branching and have found multiple endothermic peaks on melting, reflecting, the molecular segregation that occurs [37].

5. Conclusions

For crystallisation at a constant degree of supercooling the chromium material, polymer A has the fastest overall crystallisation rate followed by the metallocene catalysed polymers B and C in descending order of rate. Polymer C, a metallocene catalysed medium density polyethylene (MDPE) has a much greater supercooling range than polymer A (a chromium catalysed) and polymer B (a metallocene catalysed) MDPE, starting a few degrees below its melting temperature. Crystallisation at low temperatures did not show significant evidence for molecular segregation and reorganisational effects. Low Avrami exponents were observed mainly in polymers A and B, which did not exhibit a spherulitic superstructure. Avrami exponents representative of spherulitic development with superior nucleation habit were observed for polymer C. We suggest that the transition between these two extremes of kinetics is marked by spherulitic (or domain) impingement. We have also shown that MT-DSC is potentially capable of separating reorganisational from melting processes in the DSC but further work is required to understand the MT-DSC behaviour.

A three tier lamellar morphological hierarchy is seen in all three polymers, with lamellar domaining at the upper most level, dominant lamellar structures at intermediate length scales with fine-textured subsidiary and in-filling lamellae at the smallest scale. The melt-crystallised morphology of polymer C showed crystal thicknesses of approximately one-half of the calculated inter-branch-separation. We suspect that in our slow cooled samples the butyl branches are excluded from the orthorhombic crystal lattice. We are undertaking X-ray diffraction to investigate the influence of chain structure on unit cell

dimensions. In the broadly distributed molecular weights of polymers A and B, lamellar thicknesses were broadly in line with those expected from their melting point behaviour.

Acknowledgements

We very gratefully acknowledge the support of Fina Research, Feluy (Belgium).

References

[1] Proceedings of the International Polyethylene Conference. The Institute of Materials. The Connaught Rooms, London, UK, 3–24 October 1997.
[2] Spitz R, Saudemont T. L'Actualite Chimique 1996;4:5.
[3] Gauthier X-V. Informations Chimie 1996;375:83.
[4] Soares JBP, Kim JD, Rempel GL. Ind Eng Chem Res 1997;36:1144.
[5] D'Agnillo L, Soares JBP, Penlidis A. J Polym Sci Part A: Polym Chem 1998;36:831.
[6] Soares JBP, Hamielec AE. Polymer 1995;36:1639.
[7] Stark P. Polym Int 1996;40:111.
[8] Chemistry in Britain. February 1994. p. 87.
[9] Chemistry & Industry. November 1994. p. 857.
[10] Schellenberg J. Adv Polym Tech 1997;16:135.
[11] Parker JA, Bassett DC, Olley RH, Jaaskelainen P. Polymer 1994;19:4140.
[12] Kuwabara K, Kaji H, Horii F, Bassett DC, Olley RH. Macromolecules 1997;30:7516.
[13] Janimak JJ. Unpublished SAXS data. University of Reading, 1994.
[14] Bassett DC. Principles of polymer morphology. Cambridge: Cambridge University Press, 1981.
[15] Tanzawa Y, Ohde Y. Polymer 1998;39:3993.
[16] Hoffman JD, Weeks JJ. J Res Nat Bur Stand, Sect 1962;A66:13.
[17] Hoffman JD, Davies GT, Lauritzen Jr JI. In: Hannay NB, editor. Treatise in solid-state chemistry, vol. 3. New York: Plenum Press, 1976. p. 497–614 chap. 7.
[18] Janimak JJ, Stevens GC. Submitted for publication.
[19] Sutton SJ, Vaughan AS, Bassett DC. Polymer 1996;37:5735.
[20] Hoffman JD, Miller RL. Polymer 1997;38:3151.
[21] Ungar G, Keller A. Polymer 1986;27:1835.
[22] Cheng SZD, Zhang A-Q, Chen J-H. J Polym Sci, Part C: Polym Lett 1990;28:233.
[23] ASTM Standard D-1928-90. Preparation of compression-moulded polyethylene test sheets and test specimens.
[24] Freedman AM, Bassett DC, Vaughan AS, Olley RH. Polymer 1986;27:1163.
[25] Reading M. US Patent 5,474,385. 12 December 1995.
[26] Avrami M. J Chem Phys 1939;7:1103.
[27] Avrami M. J Chem Phys 1940;8:212.
[28] Martuscelli E, Pracella M, Volpe GD, Gerco P. Makromol Chem 1984;185:1041.
[29] Janimak JJ, Cheng SZD. Polym Bull 1989;22:95.
[30] Olley RH. Personal communication, 1998.
[31] Janimak JJ. Stevens GC. In preparation.
[32] Janimak JJ, Stevens GC. In preparation.
[33] Wunderlich B. Macromolecular physics, Crystal melting, vol. 3. New York: Academic Press, 1990.
[34] Kim M-H, Phillips PJ. J Appl Polym Sci 1998;70:1893.
[35] O'Connell PA, Bonner MJ, Duckett RA, Ward IM. Polymer 1995;36:2355.
[36] Lagaron JM, Dixon NM, Reed W, Pastor JM, Kip BJ. Polymer 1999;40:2569.
[37] Guo M, Fu Q, Cheng SZD. ACS Polymer Preprints 1997;38(2):341.